JOURNAL OF GEOPHYSICAL RESEARCH, VOL. 114, A03103, doi:10.1029/2008JA013738, 2009

Evidence for wave coupling in type III emissions

P. Henri,[1,2] C. Briand,[1] A. Mangeney,[1] S. D. Bale,[3] F. Califano,[1,2] K. Goetz,[4] and M. Kaiser[5]

Received 8 September 2008; revised 5 December 2008; accepted 23 December 2008; published 5 March 2009.

[1] Using new capabilities of waveform analyses provided by the S/WAVES instruments onboard the two STEREO spacecraft, we present for the first time a complete set of direct evidence for three-wave coupling occurring during a type III emission and involving two Langmuir waves and an ion acoustic wave. Information on the Doppler-shifted frequencies and especially the phases of the waves are used in order to check first the conservation of momentum and energy, through Fourier analyses, and second the phase locking between the waves, through bicoherence analyses. Wavelet analyses allow us to resolve for the first time the coupling regions, in which spatial length is estimated to be 18 ± 5 km. The wave packets travel at comparable speed, and the characteristic available interaction time is about 1 s. Interpretations of the phase coupling and evaluation of the growth rate of the waves tend to favor the parametric decay, at least in the observational events considered in this work.

Citation: Henri, P., C. Briand, A. Mangeney, S. D. Bale, F. Califano, K. Goetz, and M. Kaiser (2009), Evidence for wave coupling in type III emissions, *J. Geophys. Res.*, *114*, A03103, doi:10.1029/2008JA013738.

1. Introduction

[2] Solar type III radio emissions are one of the most prominent features of the meter-decameter ranges of frequency. The emissions show a pronounced drift with time toward lower frequencies (an example is shown on Figure 2). Since the early work of *Wild* [1950] and *Ginzburg and Zheleznyakov* [1958], the generally accepted model for such emission is as summarized below. During a flare, high-energy electrons (1–100 keV) are expelled from the solar corona and travel along the interplanetary magnetic field lines. They produce a bump on the local electron distribution function generating Langmuir waves via the so-called "bump-on-tail instability." Then, nonlinear wave couplings generate electromagnetic waves at f_p^- (the local electron plasma frequency) or $2f_p^-$. The plasma frequency decreases with the heliocentric distance owing to the decrease of the electron density: this is the origin of the time frequency drift characteristic of the type III emissions.

[3] However, as noted by *Sturrock* [1964], such a mechanism should deplete all the energy of the beam on a very short time scale, which would not be able to travel long distances as observed. Since then, many studies have been devoted to validate the general model and to identify the processes able to remove the particles out of resonance with the waves and that stopping the growth of the waves and allowing the beam to survive long distances.

[4] Different lines of research were developed. The first one, within the frame of the quasi-linear theory, takes advantage of the turbulent state of the solar corona and solar wind: the fast particles are moved out of resonance with the waves through scattering of the unstable waves on density fluctuations covering a wide spectrum (from a few hundred of meters to several hundred of kilometers) [*Smith*, 1970; *Li et al.*, 2006]. However, *Lin et al.* [1981, 1986] provided observational evidence that quasi-linear relaxation alone cannot explained the evolution of the beam (at least for the events they studied). First, they showed that the electric field intensity computed from the theoretical growth rate, extrapolated using the observed positive slope of the electron distribution function, would be too large. The amplitude of the waves would grow out of the framework of quasi-linear theory. Second, quasi-linear models predicts a plateauing of the bump of the distribution function which is not observed.

[5] A second line of research takes into account inhomogeneities in the solar wind density [*Budden*, 1985] through linear mode conversion and scattering of Langmuir waves on density gradients. *Willes and Cairns* [2001] and *Willes et al.* [2002] explained how Langmuir waves propagating along the density gradients can be mode converted, which could remove the beam particles out of resonance with the waves. In the Stochastic Growth Theory framework [*Robinson*, 1993], the beam driven Langmuir growth rate is treated as a random variable that depends on random density inhomogeneities, thus allowing the beam to propagate long distances.

[6] Type III electromagnetic emissions are thought to be produced via two different nonlinear wave-wave couplings.

[1]LESIA, Observatoire de Paris, Université Paris Diderot, CNRS, UPMC, Meudon, France.
[2]Dipartimento di Fisica, Università di Pisa, Pisa, Italy.
[3]Physics Department and Space Sciences Laboratory, University of California, Berkeley, California, USA.
[4]School of Physics and Astronomy, University of Minnesota, Minneapolis, Minnesota, USA.
[5]NASA Goddard Space Flight Center, Code 674, Greenbelt, Maryland, USA.

0148-0227/09/2008JA013738$09.00

Through electromagnetic coupling, a pump Langmuir wave L decays into a low-frequency LF waves and a transverse electromagnetic wave T_{fp-} at the local plasma frequency, observed as type III fundamental emission:

$$L \rightarrow T_{f_p^-} + LF \tag{1}$$

Through electrostatic coupling, the pump Langmuir wave L decays into a low-frequency LF and a daughter Langmuir wave L', which can further couple with the pump wave to generate a transverse electromagnetic wave T_{2fp-} at twice the local plasma frequency, observed as type III harmonic emission:

$$L \rightarrow L' + LF \qquad L' + L \rightarrow T_{2f_p^-} \tag{2}$$

[7] This paper focuses on the electrostatic coupling. A number of authors have claimed that the spectral analyses of the electric field in the solar wind provides some support in favor of the electrostatic decay process [e.g., *Lin et al.*, 1986; *Kellogg et al.*, 1992; *Gurnett et al.*, 1993; *Thejappa et al.*, 1993, 1995, 2003; *Thejappa and MacDowall*, 1998]. They based their conclusions on some characteristics signatures like the simultaneous occurrence of Langmuir and low-frequency waves (like ion acoustic, whistlers or lower hybrid waves), or the comparison between theoretical thresholds and the observed energy in the waves. However, as already pointed out by *Kennel et al.* [1980] and *Thejappa et al.* [1995], the simultaneous occurrence of two waves in the spectrum doesn't necessarily mean wave coupling. Indeed, the waves can be generated by particles of different energy present in a same electron cloud; an efficient three-wave coupling requires the fundamental equations of energy and momentum conservation to be satisfied:

$$\omega_1 = \omega_2 + \omega_3 \tag{3}$$

$$\vec{k_1} = \vec{k_2} + \vec{k_3} \tag{4}$$

where ω and $\vec{k}$ refer to the pulsation and wave number of the waves. When observed onboard only one spacecraft, equations (3) and (4) reduce to a single relation for the Doppler-shifted frequencies $f^{Doppler} = \omega^{Doppler}/2\pi$:

$$\begin{aligned} f_1^{Doppler} &= f_1 + \frac{\vec{k}_1}{2\pi}.\vec{V}_{SW} \\ &= (f_2 + f_3) + \frac{(\vec{k}_2 + \vec{k}_3)}{2\pi}.\vec{V}_{SW} \end{aligned}$$

leading to the following equation for resonance:

$$f_1^{Doppler} = f_2^{Doppler} + f_3^{Doppler} \tag{5}$$

Equation (5) can be directly tested from in situ measurements which combine high spectral and temporal resolution, as well as phase information. Only waveforms measurements can provide the required information. Such observations are available with the S/WAVES investigation on the STEREO mission [*Bougeret et al.*, 2007].

[8] On the basis of data obtained on 14 January 2007 by the waveform analyzer of the S/WAVES instrument onboard STEREO, evidence for nonlinear coupling between Langmuir and ion acoustic waves (also known as ion sound waves in the literature), at $\approx$80–250 Hz, occurring during a type III event are presented. Three complementary methods are employed: (1) a spectral analyses that checks the frequency correlation, (2) a wavelet analyses that verifies the time occurrence of the waves, and (3) a bicoherence analyses that checks the phase correlation between the waves. The validity of equations (3) and (4) on observed data is thus directly tested (through equation (5)). The phase relation was already studied in the Earth bow shock [*Dudok de Wit and Krasnosel'Skikh*, 1995] and the foreshock [*Bale et al.*, 1996] environments, but, to our knowledge, it is the first time it is used on data related to type III event. This paper focuses on the parametric instability version of the electrostatic decay, through direct tests on the phase resonance, rather than its weak turbulence version [*Robinson et al.*, 1993]. This will be justified by the bicoherence analysis of the electric waveforms.

[9] Details on the instrument, the data and the solar wind conditions are presented in section 2. After identification of the low-frequency mode, three independent analyses for the three-wave coupling are presented in section 3. Section 4 discusses details on the coupling and describes it in the context of the type III.

2. Observations and Data

[10] S/WAVES is composed of three 6 m monopole antennas, orthogonal to each other, with an effective length of about 1 m [*Bougeret et al.*, 2007; *Bale et al.*, 2008]. Two modes of observation are available: remote sensing to follow the propagation of the radiosources in the solar wind with spectral radio receivers and *in situ* measurement of electric waveforms along the three antennas with the Time Domain Sampler mode (TDS).

[11] The TDS data reported in this paper are composed of N = 16384 samples with an acquisition rate of 125,000 samples per second (a time step of δt = 8 μs for a total duration of 130 ms per event). This long total duration allows us to capture entire Langmuir wave packets. In terms of frequencies, those electric field waveforms enable to cover a range from 10 Hz to 60 kHz. Thus, signatures from below the electron cyclotron frequency (typically 100 Hz in the solar wind) to above the plasma frequency (typically 10 to 20 kHz) are accessible. The frequency gain is flat in the frequency range of interest here (100 Hz to 20 kHz). Finally, the S/WAVES A/D converter is accurately linear. Thus spurious nonlinear artifacts are not introduced, so that studies of nonlinear wave interactions are possible.

[12] The voltage measured on the three antennas is then converted into an electric field, and projected in the spacecraft coordinates, using the set of parameters called w/base caps (Graz) by *Bale et al.* [2008, Table 13] in order to take into account the effective length and direction of the STEREO antennas.

[13] In its final orbit the spacecraft coordinates (X, Y, and Z) are defined as follows: the x component is sunward along the radial direction, the Z component is normal to the ecliptic plane, southward for STEREO A and northward

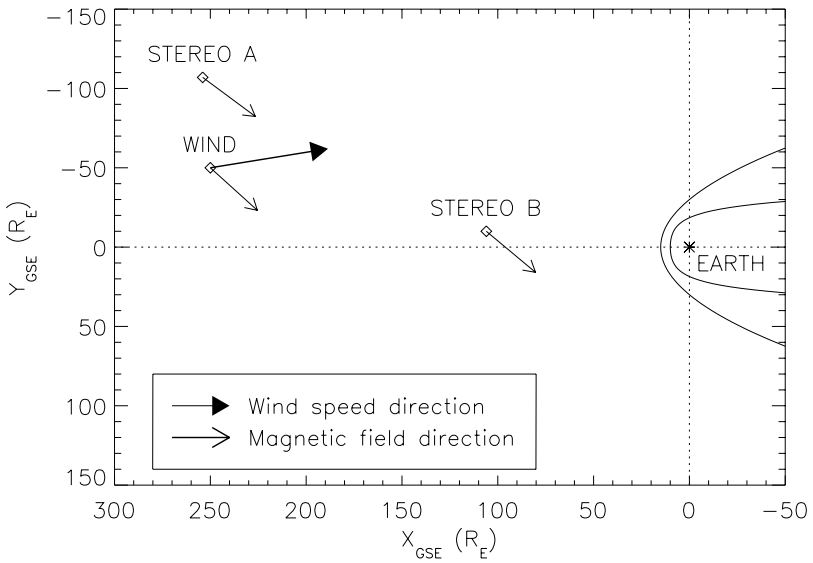

Figure 1. Position of WIND and STEREO A and B projected on the ecliptic plane in GSE coordinates on 14 January 2007 when the type III solar burst reaches the spacecraft. Distances are expressed in Earth radii (R_E) units. The solar wind speed and the magnetic field direction recorded by the spacecraft are displayed. The values of the magnetic field magnitude and angle with the solar wind direction are discussed in the text.

for STEREO B, and the Y component complete the direct orthogonal frame. But by the day considered in this study, both STEREO spacecraft were not yet in their final orbit. They were slowly rotating around the radial direction, to reach their final configuration. Thus, the spacecraft coordinates are corrected as follows: the x component is indeed sunward in the radial direction, but the Y and Z components are rotated by an angle of about $-90°$ compared to the previous definition on STEREO A and 180° on STEREO B. In the following, the electric field measurements are expressed in the corrected spacecraft coordinates.

[14] Figure 1 displays the position of WIND, STEREO A and STEREO B on 14 January 2007, together with magnetic field and wind speed directions. The spacecraft are separated by less than 200 Earth radii, so that plasma measurements from WIND are used when those from STEREO are not available (wind speed, temperatures). The 1 h average wind speed from WIND/3-DP [*Lin et al.*, 1995] is about $V_{SW} = 315$ km s^{-1}. The magnetic fields are recorded by IMPACT [*Acuña et al.*, 2007] at 8 samples s^{-1} onboard both STEREO and by MFI [*Lepping et al.*, 1995] onboard WIND with 3 s resolution. The amplitude of the magnetic field is 7.4 nT at STEREO A, 7.3 nT at STEREO B, and 7.4 nT at WIND with maximal fluctuations below 0.2 nT during the period of interest. The magnetic field and wind speed directions, obtained from WIND data with 92 s resolution values, make an angle $\theta = 60°$ with maximal fluctuations below 9 during this period. The magnetic field direction is almost identical at the three spacecraft positions and remains constant within a few degrees during the whole period of interest.

[15] The electron temperature observed by WIND/3DP is $T \simeq 10^5$ K, and the electron density in the solar wind, estimated from the plasma frequency, is about $n \simeq 10^6$ m^{-3}. From the electron density and temperature, the Debye length is $\lambda_D \simeq 10$ m.

[16] Figure 2 displays the time-frequency spectrum (the so-called dynamic spectrum) recorded by WIND/WAVES (WIND has higher sensitivity than STEREO for distinguishing the plasma line) between 0700 and 1500. Type III is observed from 1040 to 1150 (UT). The drift of the fundamental (full line) and the harmonic (dashed line) radio emissions are estimated from the onset time of the type III and the Parker spiral (Estimation courtesy of S. Hoang following *Hoang et al.* [1994]). The radio emission in this event is dominated by the harmonic while the fundamental is very weak. An enhanced level of Langmuir wave activity appears when the extrapolated fundamental of the type III intersects the local (satellite position) plasma frequency line (at about 1110 (UT) on WIND). Assuming that the beam travels along the Parker spiral, the estimation of the onset time of the type III, together with the observed onset time of Langmuir wave activity, leads to an estimation of the electron beam speed associated with the type III of about $V_b \simeq 0.21c$. The Langmuir activity was also recorded by the in situ measurements of S/WAVES/TDS, as a signature of the type III electrons passing the spacecraft. Note that owing to ballistic effects, the type III electrons should cross the three spacecraft at different times. In the following, we concentrate on the TDS Langmuir events associated with this type III on STEREO A between 1125 and 1205 UT, and on STEREO B between 1150 and 1215 UT. Nineteen such events have been measured by STEREO A and 26 events by STEREO B.

[17] Other type III bursts are recorded by WIND/WAVES before and after the one we study. No TDS electric field waveforms associated with these bursts have been telemetered, possibly because of criteria selection from the TDS or because the electron beams associated with these bursts may not have crossed the STEREO spacecraft. Thus, they are not described in the present paper.

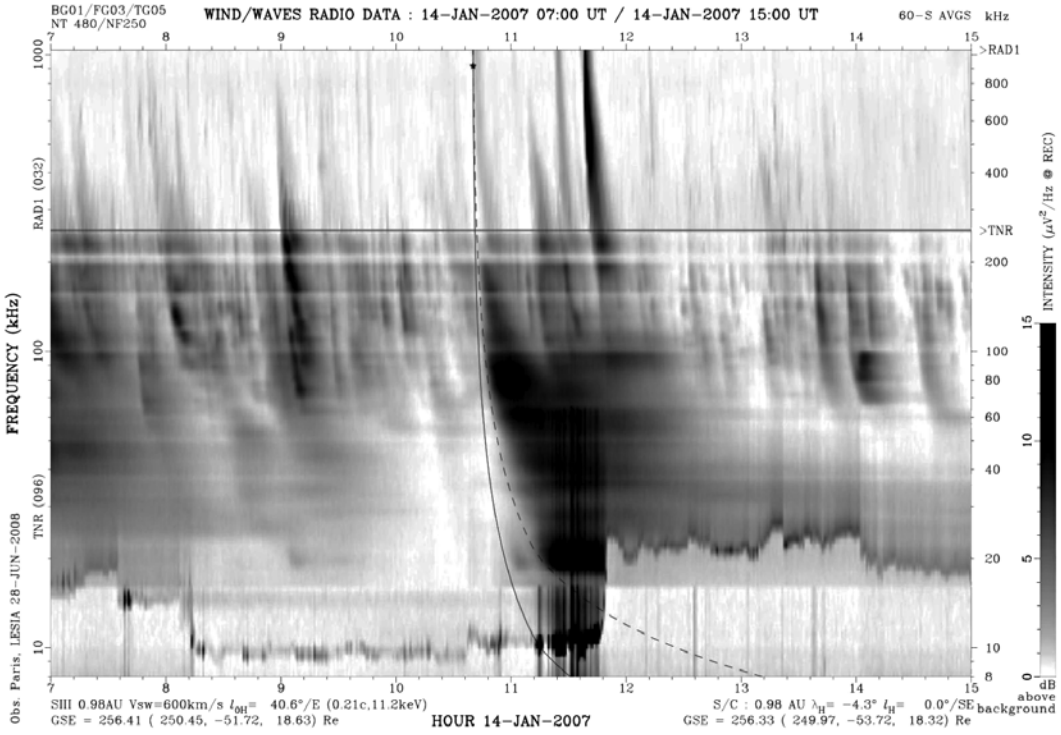

Figure 2. Time frequency spectrum from WIND/WAVES on 14 January 2007. A type III burst is observed from 1040–1150 (UT). The full line shows the leading edge of the fundamental emission. The dashed line corresponds to the leading edge of the harmonic emission. Courtesy of S. Hoang.

[18] Moreover, since the fundamental electromagnetic emission was not observed in this type III burst, the electromagnetic coupling mechanism, see equation 1, for generating the fundamental radio emissions at the plasma frequency is out of the scope of this paper.

3. Evidence for Wave Coupling

[19] Figure 3 shows the three components of the electric field of a typical event. An entire beat-like wave packet is captured, lasting 50 ms. The maximal intensity of the electric field is of the order of 10 mV m^{-1}, the amplitude along the X direction being larger than the two other components.

3.1. Spectral Analyses

[20] Figure 4 displays the Fourier spectrum of the x component of the electric field for the event shown on Figure 3. Three main features appear: a low-frequency peak at 0.25 kHz, an small intermediate frequency peak at 3 kHz, and a high-frequency peak at 10 kHz. This last frequency is identified from the dynamic spectrum (Figure 2) as the local plasma frequency f_p^-, and corresponds to the Langmuir waves. A closer view on the high-frequency signal (Figure 4, bottom) shows that it is actually composed of two peaks separated by 0.25 kHz. The difference between the frequency of the two Langmuir waves matches the lower frequency. We now focus on the identification of the low-frequency wave.

[21] The electron cyclotron frequency is about 0.2 kHz, i.e., in the frequency range where the LF signal is observed. The LF wave could be electromagnetic waves, such as whistler and lower hybrid waves, or electrostatic waves such as electron Bernstein mode or ion acoustic waves.

[22] When filtering out the high-frequency component, the LF signal appears as a modulated sine-like function identical on the three antennas. This could be interpreted as the signature of a longitudinally polarized wave along the bisectrix of the three antennas (the X direction), but since this direction is related to the spacecraft geometry and is usually different from the solar wind speed or the magnetic field directions, such an explanation is very unlikely. However, as pointed out by *Kellogg et al.* [2007], the signal can be dominated at low frequencies by local density fluctuations in which the spacecraft is embedded (through quasi-static modifications of the spacecraft charging). In this case, the response is expected to be identical on the three antennas and the signal would appear only on the x component, when "projected" in the spacecraft coordinates.

[23] The LF signal is thus identified as density perturbations associated with a LF wave. Among the candidates in this range of frequency, the only wave mode associated with density fluctuations is the ion acoustic wave (IAW). Indeed, when observing the other waves, which density fluctuations are negligible, the recorded signal should be dominated by the electric field, rather than by density fluctuations, thus showing different signals on the three antennas, which is not observed. We thus identify the low-frequency signature as an IAW.

[24] Let us stress that we observe the IAW density fluctuation in terms of an "equivalent" electrical field. The true IAW electric field is proportional to and in phase quadrature with the observed potential generated by the

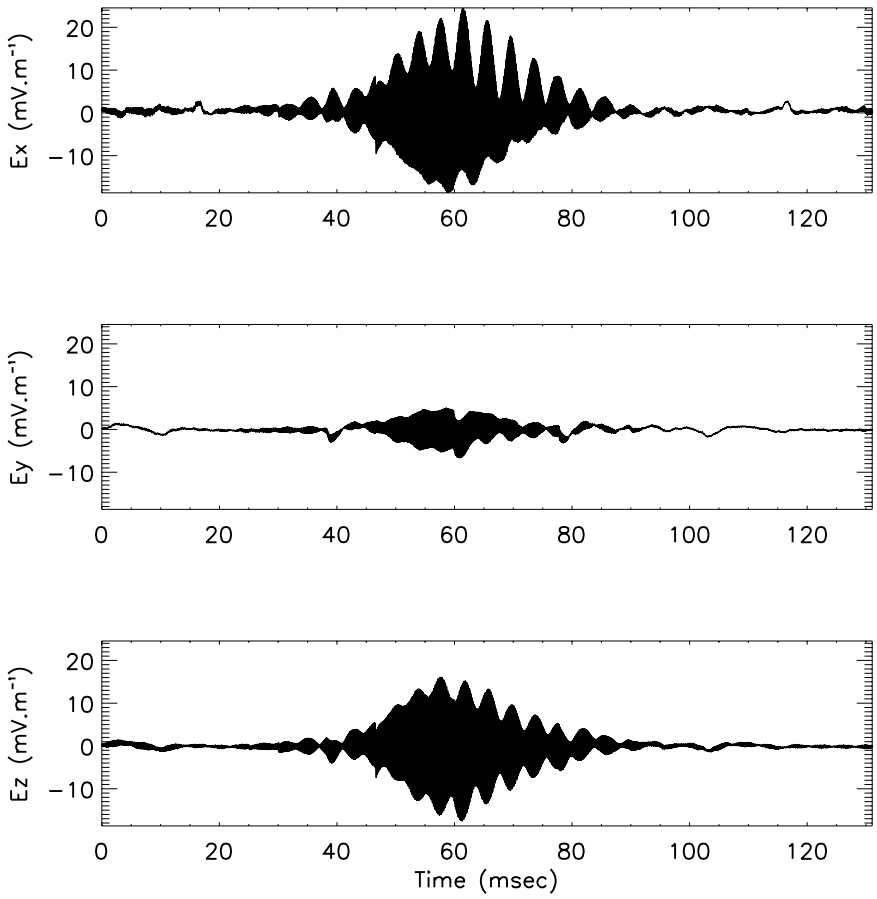

Figure 3. Typical electric field waveform of Langmuir waves recorded by S/WAVES/TDS in spacecraft coordinates, associated with type III.

IAW density fluctuation. From now on, we will work only with the x component electric field, and we consider the density fluctuations as a tracer for IAW electric field.

[25] During the period of strong Langmuir activity, a total of 37 TDS events (19 from STEREO A and 18 from B) were transmitted from the two spacecraft. Among these events, 14 (10 on STEREO A and 4 on B) show two distinguishable Langmuir wave peaks together with an IAW. Figure 5 displays for each event the relation between the frequency difference Δf_L between the two Langmuir waves and the frequency f_{IA} of the IAW for the two spacecraft. The resonant relation $\Delta f_L = f_{IA}$ is very well satisfied for all 14 events. This relation between frequencies observed in the spacecraft frame is compatible with the conservation of momentum and energy that must be satisfied in case of three-wave coupling (equation 5) and strongly suggests the possibility of such a nonlinear wave coupling. In order to confirm this three-wave coupling, we use two different analyses: a wavelet analyses (section 3.2) and a bicoherence analyses (section 3.3) are now considered on these selected TDS events.

3.2. Wavelet Analyses

[26] The wavelet transform is a powerful method to study a signal composed of nonstationary waves [*Daubechies*, 1990; *Farge*, 1992].

[27] Consider a time series E_n with time step δt, the wavelet transform of the time series is defined as the convolution of the signal with a "mother" wavelet function ψ normalized, translated, and scaled (s being the scale):

$$W_n(s) = \sum_{n'=0}^{N-1} E_{n'} \frac{1}{\sqrt{s}} \psi^* \left(\frac{(n'-n)\delta t}{s} \right)$$

where ψ^* stands for the complex conjugate of ψ. Among various wavelets, we choose the Morlet wavelet Ψ_0, consisting of a plane wave modulated by a gaussian envelope:

$$\Psi_0(\eta) = \pi^{-1/4} e^{i2\pi\eta} e^{-\eta^2/2}$$

With this definition, the Morlet wavelet scale factor s is equal to the inverse of the Fourier frequency, which simplifies the interpretation of the wavelet analyses. The Morlet wavelet is known to provide a good compromise between time and frequency resolution (reviews on wavelet analyses can be found in the work by *Torrence and Compo* [1998] and *van den Berg* [1999]).

[28] Figure 6 displays the modulus of the wavelet transform applied to the waveform displayed in Figure 3 (top). The resolution in frequency of the Morlet wavelet transform

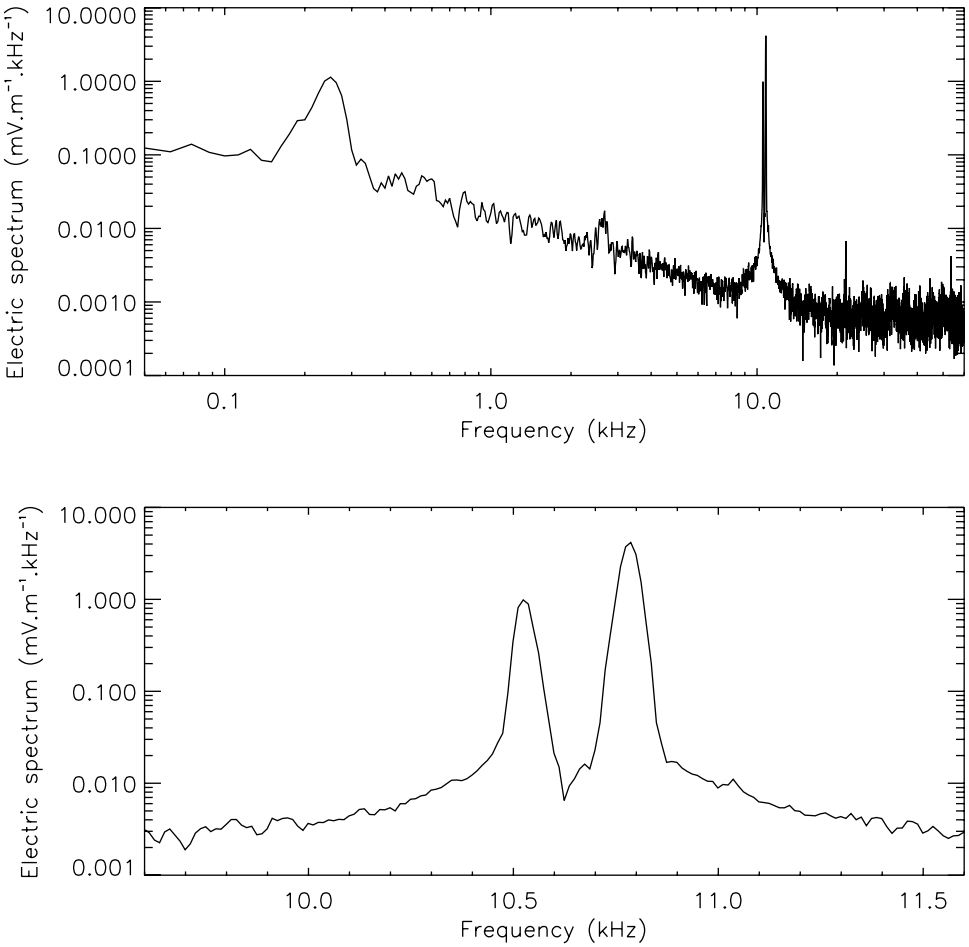

Figure 4. Fourier spectrum of the x component electric field from Figure 3. (top) Whole frequency range. (bottom) Zoom centered on the high-frequency double feature at 10 kHz.

is not sufficient to separate the two high frequencies at about 10 kHz. Instead it shows a signal, at the average of these two frequencies, modulated by the beating frequency. The IAW at 0.25 kHz is maximum at 60 ms when the maximum of the Langmuir waves occurs.

[29] This is a general feature: a systematic wavelet analyses on the 14 events reported in Figure 5 shows indeed that the IAW and the Langmuir signals always occur simultaneously. Knowing the electron temperature, the ion sound speed is estimated to be $C_s \simeq 30$ km.s^{-1}. Since the solar wind speed $V_{SW} \simeq 315$ km.s^{-1}, the IAW packets are mainly advected by the solar wind flow. From the average duration of the IAW packets, the spatial length of the IAW packet is estimated to be $\sim 18 \pm 5$ km. Note that the 3 kHz signal is present during all the event, but is not correlated with the two Langmuir waves, neither with the IAW.

3.3. Bicoherence Analyses

[30] Up to now, we have focused on the simultaneous occurrence of three waves, with frequencies consistent with a three-wave nonlinear coupling. But coupling requires also phase coherence between the waves. Such phase relations can only be checked from waveform data.

[31] The bicoherence is used as an estimator of quadratic phase coupling, characteristic of three-wave coherent interactions. *Lagoutte et al.* [1989] give a methodological introduction to bicoherence analyses based on a Fourier approach. Although studies of bicoherence have been reported in the ionosphere [*Pecseli et al.*, 1993], the bow shock [*Dudok de Wit and Krasnosel'Skikh*, 1995] and the solar wind near the foreshock edge [*Bale et al.*, 1996], to our knowledge, the present analyses represents the first time that bicoherence is used to study three-wave coupling in the solar wind during a type III.

[32] In the case of three-wave coupling, the relative phase $\Phi_1 + \Phi_2 - \Phi_3$ between the three phases $\Phi_{i=1,3}$ associated to the three frequencies $f_{i=1,3}$ linked by the relation $f_1 + f_2 = f_3$ should remain constant. Bicoherence measures statistically the degree of stationarity of this relative phase.

[33] To optimize the time resolution, and diminish the bias introduced by the method, the wavelet bicoherence [*Van Milligen et al.*, 1995; *Dudok de Wit and Krasnosel'Skikh*, 1995] is here preferred to the Fourier bicoherence. For convenience, the wavelet transform will thereafter be expressed in terms of frequencies, instead of scales. The wavelet cross bispectrum is defined in frequency space as

$$B(f_1, f_2) = < W(f_1) W(f_2) W^*(f_1 + f_2) > \qquad (6)$$

where $< >$ stands for the average over the samples, and W^* for the complex conjugate of W (recall that $W(n\delta t, F = 1/s)$ is a function of both time and frequency).

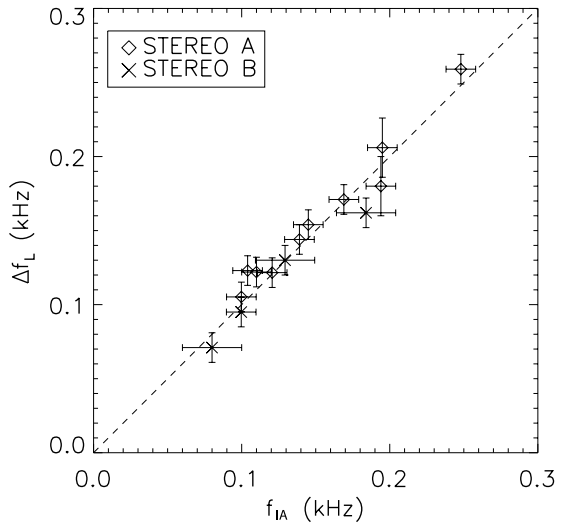

Figure 5. Difference between the two Langmuir frequencies (Δf_L) as a function of the ion acoustic wave frequency (f_{IA}) on 14 different events on STEREO A and B. Each point represents a different Time Domain Sampler (TDS) event during the type III. Only events showing an ion acoustic mode and two Langmuir waves are displayed. The dotted line is not a fit but shows the expected identity $\Delta f_L = f_{IA}$.

[34] To take into account phase effects only, in other words to avoid amplitude effects, the wavelet cross bispectrum is normalized. The wavelet normalized cross bispectrum, also called wavelet bicoherence, is thus defined as

$$b(f_1,f_2) = \frac{< W(f_1)W(f_2)W^*(f_1+f_2) >}{< |W(f_1)W(f_2)W^*(f_1+f_2)| >}$$

For a stationary signal, the bicoherence vanishes when the phase relation is random, and maximal (1 for the chosen normalization) when the phase relation remains constant. A nonzero bicoherence value $b(f_1, f_2)$ is thus the signature of phase locking between three waves with frequencies f_1, f_2, and $f_1 + f_2$.

[35] When using a wavelet basis, the bicoherence is computed by averaging on overlapping samples. But as stressed by *Soucek et al.* [2003], the statistical validation of bicoherence requires to use independent samples. The duration of an independent sample can be evaluated from the time of coherence of the waves, which is about the duration of the wave packet. It means that each TDS event should be considered as an independent sample and that the bicoherence computed with only one event can be meaningless.

[36] Bicoherence is very sensitive to the nonstationarity of frequencies and to the presence of discontinuities in the data set. The nonstationarity of frequencies involved in a three-wave coupling spreads the bicoherence signal and thus decreases the wavelet bicoherence value at all involved frequencies. This is a consequence of the intrinsic frequency accuracy of the Morlet wavelet. Indeed, the time-frequency finite resolution of the chosen wavelet implies that the uncertainty on the frequencies is $\Delta F \simeq 1/4f$, with Δf the resolution at 3 dB. Discontinuities in the waveform, such as spikes, appears through spectral analyses as a large spectrum of coupled frequencies (for instance Dirac's function is a white noise with correlated phases). This implies an increase of the bicoherence signal, without physical significance, and thus reduces the signal-to-noise ratio of the bicoherence. To avoid both effects, only events with an IAW in the frequency range (100 Hz, 200 Hz), and free of spikes are considered, reducing the number of useful samples to 10. The signal analyzed for the study of bicoherence resulted from the concatenation of these 10 "independent"

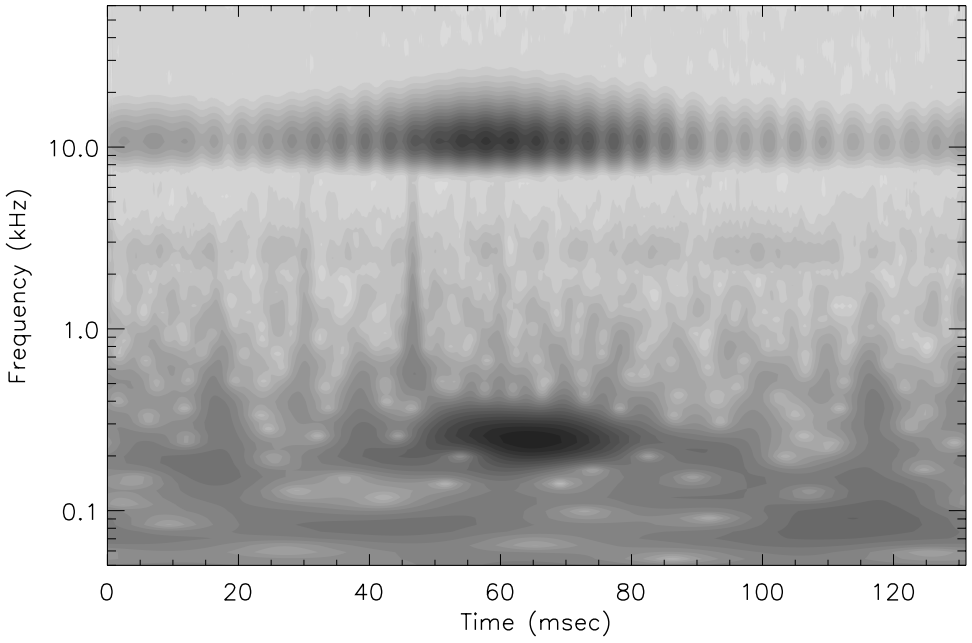

Figure 6. Modulus of the Morlet wavelet transform of the event displayed in Figure 3 (top).

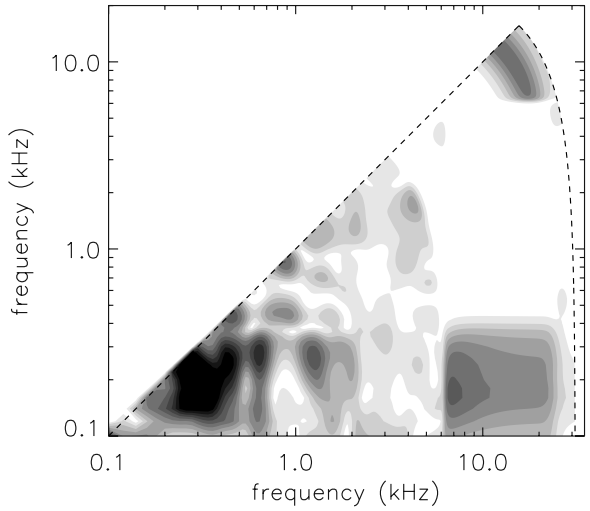

Figure 7. Wavelet bicoherence of three-wave TDS events computed for frequencies from 100 Hz to 30 kHz (inside the dotted line). Minimum value in white for bicoherence $b = 0$, maximum value in black for bicoherence $b = 0.6$. Note three main signatures at $(f_{IA}, f_{IA}) \simeq$ (0.2 kHz, 0.2 kHz); $(f_L, f_L) \simeq$ (10 kHz, 10 kHz) and $(f_L, f_{IA}) \simeq$ (10 kHz, 0.2 kHz).

samples, the averages appearing in equation (6) being replaced by averages over the points of the concatenated signal.

[37] Note that the density fluctuation of the IAW is in phase quadrature with its associated electric field, which does not affect the bicoherence study because bicoherence is not sensitive to constant dephasing.

[38] Figure 7 shows the results of the bicoherence analyses computed in this way. Three main signatures linked to the three waves discussed above arise at $(f_{IA}, f_{IA}) \simeq$ (0.2 kHz, 0.2 kHz); $(f_L, f_L) \simeq$ (10 kHz, 10 kHz); $(f_L, f_{IA}) \simeq$ (10 kHz, 0.2 kHz). The evaluation of the statistical significance of the bicoherence, discussed bellow, shows that the multiple signatures at frequencies lower than 6 kHz are significant. However, it is not linked to the three-wave process discussed in this paper and will described in a future work. We limit the present discussion to the following results.

[39] First, at low frequencies, the phase resonance between low-frequency modes at $(f_{IA}, f_{IA}) \simeq$ (0.2 kHz, 0.2 kHz) can be interpreted as the generation of harmonics of the IAW. It could also be linked to the multiple bicoherence signatures present in this frequency range. However, no obvious peak at twice the IAW frequency is seen in the Fourier spectrums.

[40] Second, the bicoherence shows a phase locking that involves waves at about 10 kHz. This could be interpreted as the generation of the transverse EM mode at $2f_p$ generated during the type III. However, the conversion of Langmuir waves into EM waves $L + L' \rightarrow T$ should be hard to detect because of the low sensitivity of the antennas to local EM waves. The observed bicoherence signature is more likely due to the generation of the Langmuir harmonics at twice the plasma frequency. The bicoherence value is $b(f_L, f_L) = 0.34$.

[41] Third, the main result of this bicoherence analyses is the evidence for a bicoherence signal that involves a high-frequency mode $f_L \simeq 10$ kHz and a low-frequency mode $f_{IA} \simeq 0.1-0.2$ kHz, with a value of $b(f_L, f_{IA}) = 0.37$. Indeed, this implies that the three waves described in sections 3.1 and 3.2 remain phase locked from one event to the other. It is the signature of the expected phase coupling between the IAW and the two Langmuir waves. This is a strong evidence in favor of three-wave interaction in agreement with the hypothesis suggested by Fourier and wavelet analyses.

[42] To validate the bicoherence study, one can evaluate the statistical threshold above which the bicoherence applied to the original signal is considered significant, by computing the bicoherence on phase randomized surrogate data. Surrogate data are generated from the original data set by keeping the power spectrum unchanged and redistributing the phases randomly, in order to destroy the nonlinear dynamics in the data. See *Koga and Hada* [2003] and *Siu et al.* [2008] for details on the method. Bicoherence computed on 30 phase randomized surrogates (a good compromise between statistics and computing time) shows in the frequency domain of interest a mean bicoherence response $\bar{b} < 0.04$, with a standard deviation $\sigma_b < 0.03$. Bicoherence computed on the original data with response above $\bar{b} + 3\sigma_b \simeq 0.1$ are thus considered significant. This result clearly confirms the validity of our bicoherence analyses, thus demonstrating the three-wave coupling.

4. Discussions

[43] We have shown that the data obtained on 14 January 2007 by the waveform analyzer of the S/WAVES instrument onboard STEREO, show strong evidence for a nonlinear coupling between two Langmuir waves and an IAW in the range 80–250 Hz. The IAW observed frequency is dominated by the Doppler shift; its wavelength is estimated between 1 and 3 km for the different events. From conservation of momentum, the wavelengths of the Langmuir waves are about twice this value. Considering that the spatial length of the coupling region is of the order of the length of the advected ion acoustic wave packet, we estimate the average spatial length L_c of the coupling region to be $L_c \sim 18 \pm 5$ km (about 2.10^3 λ_D). As a result, the length of the coupling zone, as discussed in section 3.2, is quite short since it only covers a few Langmuir wavelengths. We shall now come to discuss the nature of the coupling as well as the consequences for the understanding of the physics of type III bursts.

4.1. Electrostatic Coupling

[44] The bicoherence analysis shows a phase resonance between the three waves. Therefore, we interpret the observed coupling between electrostatic waves in term of a parametric instability rather than the weak turbulence approach.

[45] The observed electrostatic three-wave coupling can be explained via two kinds of parametric coupling. The first one concerns the parametric decay of a finite-amplitude Langmuir wave (L) into an IAW (S) and a backscattered daughter Langmuir wave (L'):

$$L \rightarrow S + L'$$

The second one concerns the scattering of a beam excited mother Langmuir wave by preexistent IAW into a backscatter Langmuir wave:

$$L + S \rightarrow L'$$

[46] In the case of parametric decay, the IAW is expected to be generated by the ponderomotive force created by the two beating Langmuir waves. The electric pressure is thus expected to compensate the thermal pressure. To test this possibility, the ratio of electric energy to thermal energy is

$$\frac{\epsilon_0 E^2}{n k_B T} \simeq 6.10^{-4}$$

using the following values: $E \simeq 10$ mV.m^{-1} the observed electric field for the Langmuir waves, $T \simeq 10^5$ K the electron temperature and $n \simeq 10^6$ m^{-3} the electron density. The threshold for parametric decay of the pump Langmuir wave into a daughter Langmuir wave and an IAW is [*Nishikawa*, 1968; *Bardwell and Goldman*, 1976]

$$\frac{\epsilon_0 E^2}{n k_B T} > 8 \frac{\gamma_{IA}}{\omega_{IA}} \frac{\gamma_{L'}}{\omega_{L'}}$$

with ω and γ the angular frequency and Landau damping of the IAW and daughter Langmuir waves. The threshold for electrostatic decay has been estimated for typical solar wind parameters to be $\frac{\varepsilon_0 E^2}{n k_B T} \geq 2.5\ 10^{-5}$ [*Lin et al.*, 1986]. The observed ratio is much higher than this threshold, which allows the development of parametric decay. Since the parametric decay is far more efficient than the parametric scattering, we conclude in favor of the decay.

[47] To take into account the limited size of the wave packets, we shall now estimate whether the daughter waves have enough time to be generated via the decay process before leaving the region of the pump Langmuir wave packet. We compare the characteristic growth rate for the parametric decay to the available interaction time before the daughter wave packets leave the coupling region.

[48] First, the efficiency of the coupling requires that the ion acoustic speed matches the Langmuir wave group velocity. The IAW packets travel at the ion sound speed $C_s \simeq 30$ km.s^{-1}, and the Langmuir wave packets travel at its group velocity V_g^L, given by $V_g^L = \partial\omega/\partial k \simeq 3k\lambda_D v_e^{th}$ evaluated to $V_g^L \simeq 30$ to 100 km.s^{-1} for Langmuir wavelength $\lambda_L \simeq 2$ to 6 km. Thus both the beam-driven Langmuir wave and the ion acoustic wave packets travel at comparable speed, enabling energy transfer between the waves providing that the growth rate for the decay is large enough.

[49] Then, the available interaction time τ_I for the three waves to resonate is estimated by considering the time for which the pump Langmuir wave packet L and the backscatter Langmuir daughter wave packet L' remain inside the same region of length L_c:

$$\tau_I \sim L_c / V_g^L \sim 1\ s$$

This available interaction time for coupling is then compared to the characteristic growth time of the daughter waves. The growth rate ν for electrostatic decay in the case of monochromatic waves in an homogeneous background is [*Sagdeev and Galeev*, 1969]

$$\nu \simeq k_{IA} C_s \left(\frac{\epsilon_0 E^2}{n k_B T} \frac{m_p}{m_e} \right)^{1/4} \sim 200\ \text{s}^{-1}$$

The growth rate for electrostatic decay is evaluated to 200 s^{-1}, which is about the ion acoustic time. The available interaction time for coupling is far larger than the evaluated growth time of the daughter waves

$$\tau_I >> 1/\nu,$$

which enable the decay to develop before the daughter wave packets leave the region of coupling. The growth rate for electrostatic decay has been evaluated for infinite waves in a homogeneous medium, and gives a first order of magnitude, but the nonmonochromatic nature of the wave packets should be taken into account. Let us now describe the electrostatic coupling in the context of the type III burst.

4.2. Three-Wave Coupling and Type III Burst

[50] The main picture is the following: during a type III, electron beams generate the mother Langmuir wave through beam instability. It then decays into a backscattered daughter Langmuir wave and an IAW with proper wave numbers and frequencies given by momentum and energy conservation (equations (3) and (4)).

[51] If this Langmuir mother wave couples to a second Langmuir wave and the IAW, the relation between the frequency f_{IA} of the IAW and the speed of the electron beam is given to a good approximation by *Cairns and Robinson* [1992] and *Hospodarsky and Gurnett,* [1995]

$$V_b \approx \frac{2 f_p V_{SW} |\cos\theta|}{f_{IA}} \tag{7}$$

The beam speed for the fastest electrons involved in the coupling and observed by the TDS can be estimated from the minimum IAW frequency observed at 80 Hz at the beginning of the type III on STEREO B, together with equation (7):

$$V_b \simeq 4\ 10^5\ \text{km.s}^{-1} \simeq 0.13\ c$$

which is consistent with the estimation in section 2 from the dynamic diagram of type III (Figure 2).

[52] Simple time-of-flight arguments on the type III electron beam predict that at a given position, the beam speed V_b vary inversely with time (fast electrons cross the spacecraft first, the slower ones come after):

$$V_b \simeq D/(t - t_0) \tag{8}$$

with D the distance between the generation of the beam at t_0 and the fixed observer. *Lin et al.* [1981] observed this drift and explained how it controls the frequency drift of the beam-generated Langmuir wave. With equation (7) the IAW frequency (equal to the difference of frequency

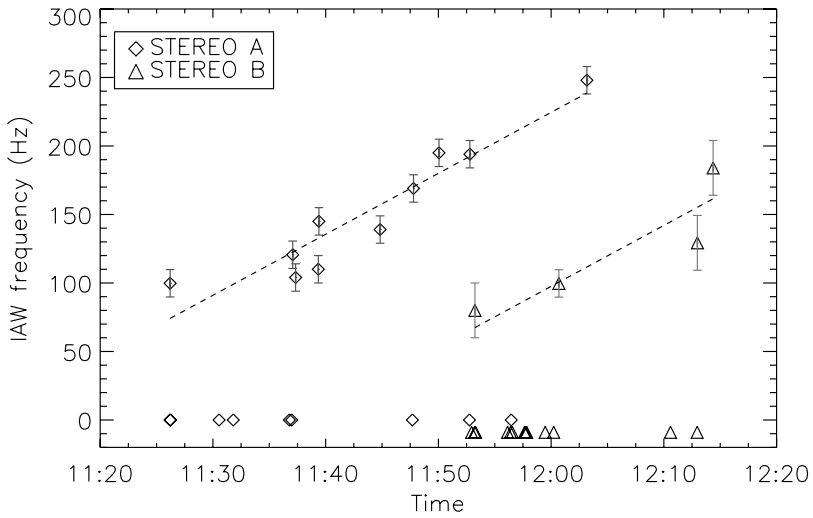

Figure 8. Ion acoustic wave frequency (f_{IA}) versus time of the event (UT). Each single event is represented by a diamond for STEREO A and a triangle for STEREO B, together with their respective error bars. The dashed line displays the least squares fit. Points at bottom ($f_{IA} \simeq 0$) show events without coupling. (For sake of clarity, STEREO B events have been shifted downward. In these last cases no IAW is reported.)

between the two Langmuir waves) is expected to vary linearly with time:

$$f_{IA} = \Delta f_L \approx \frac{2 f_p V_{SW} |\cos\theta|}{D}(t - t_0) \tag{9}$$

[53] *Cairns and Robinson* [1992] and *Hospodarsky and Gurnett* [1995] used electron distribution function measurements on different type III observed at 1 AU and derived values for the drift of the IAW frequency of 100 to 300 Hz.h^{-1} depending on the plasma parameters. Distribution functions are not yet available on STEREO and we cannot fit the beam speed drift by equation (7), so that the distance parameter D is still unknown. But a crude estimation of D $\approx$ 1 AU can be made, to get an order of magnitude of about 100 Hz.h^{-1} for the expected frequency drift.

[54] The observed IAW frequency are considered for each single event, and then plotted against the time of the event on Figure 8. Over the 14 three-wave events, the observed time variation, from one event to another, of the IAW frequency is well represented by a linear drift of 260 $\pm$ 30 Hz.h^{-1}, consistent with the time evolution of an IAW coupled with the beam-driven Langmuir wave. Since $\Delta f_L = f_{AI}$, at the same time, the two Langmuir peaks have frequencies that move away one from the other, with the same drift (not shown in the paper). This frequency drift of the IAW together with the separation in frequency of the Langmuir waves is another evidence for wave coupling in the context of the type III.

[55] Previous observations of electron distribution functions during type III also allowed the derivation of the beam velocity and the beam temperature. From these measurements *Cairns and Robinson* [1995] predicted a relative bandwidth for IAW $\Delta f_{IA}/f_{IA}$ ranging from 5% to 40%, but had not the frequency resolution to check it. Fourier analyses of the S/WAVES/TDS waveforms enables to measure it directly: $\Delta f_{AI}/f_{AI} \simeq 20\%$, which is compatible with previous observations of type III electron beams. These two last results should however be checked in the future from STEREO distribution function observations, when available.

[56] Finally, the eventual coalescence of the two Langmuir waves into a transverse wave T

$$L + L' \rightarrow T_{2f_p}$$

could then explain the generation of the type III radio harmonic emission at twice the plasma frequency observed on Figure 2 [*Ginzburg and Zheleznyakov*, 1958]. However, this mechanism was not detected in this study because of the presence of electrostatic harmonic Langmuir waves at twice the plasma frequency that prevent the direct detection of less intense transverse electromagnetic waves from *in situ* measurements.

5. Conclusion

[57] This paper shows for the first time, to our knowledge, a complete set of direct evidence of the coherent coupling between Langmuir waves and ion acoustic waves during a type III emission. The work is based on three independent methods: Fourier, wavelet, and bicoherence analyses of the S/WAVES waveform data (TDS observation mode).

[58] More than a third of the electric field data shows beam-driven Langmuir waves coupled with a second Langmuir wave and an ion acoustic wave. (1) The Doppler-shifted frequencies of the three waves satisfy the resonant relations expected for three-wave coupling. (2) The relative phase between the three waves remains constant from one waveform to another, consistent with a coherent wave-coupling mechanism. (3) The coupling regions are spatially localized with size of about 20 km, corresponding to about 2000 Debye lengths. (4) The electric field of the beam-

driven Langmuir wave is above the threshold for parametric decay. (5) By defining the interaction time as the time before interacting wave packets separate, we found that the interaction time is long enough when compared to the inverse of the excited mode growth rate. (6) The frequency of the ion acoustic waves drifts in time during the whole type III, as consistent with the expected evolution of the type III electron beam speed. This confirms the interpretation of the data in terms of the parametric electrostatic decay of the beam-driven Langmuir waves.

[59] Waveform data of S/WAVES give access to both phase information and high-frequency resolution which cannot be obtained by spectral instruments. It is worth noting that, for the first time in solar wind observations, long time series of waveform data are available. This allows us first to observe low frequencies (around 100 Hz), and second to resolve the entire coupling region. Finally, the possibility to compute time-frequency analyses with high temporal and spectral resolution enable to discriminate among the observed waves which ones are actually involved in the coupling process. For instance the 3 kHz IAW (Figure 3), frequently seen in our waveforms during the observed time of interest, but totally independent to the observed coupling, could have been thought to participate to the coupling through spectral observations only.

[60] Important questions still remain open. For example: why do the beam-driven Langmuir fluctuations appears as short isolated wave packets? *Ergun et al.* [2008] have recently shown that gaussian-shaped and modulated solar wind Langmuir waves commonly recorded in the solar wind can be interpreted trapped eigenmodes in density structures. The trapping of beam-driven Langmuir waves in density cavities, not observed but not excluded in the events studied here, could explain their spatial shape. An other possible approach could be that of beam-plasma interaction in an inhomogeneous media [*Krasnoselskikh et al.*, 2007].

[61] Another related question concerns the efficiency of the parametric decay for a nonmonochromatic pump wave. What is the evolution for the parametric decay for a short isolated Langmuir wave packet? Therefore, our model of monochromatic wave in an homogeneous media must be considered as a first step in the line of interpreting observational type III data. Numerical simulations are expected to be of great help in elucidating this nonlinear, inhomogeneous problem.

[62] The present study is based on a single type III burst, for which radio electromagnetic waves were detected from remote sensing measurements together with electrostatic Langmuir waves detected by in situ measurements. A statistical analysis will certainly be possible during the growing phase of the current solar cycle, when more events are observed, to offer more observational constraints on the theory.

[63] **Acknowledgments.** The authors thank S. Hoang for his work on the type III dynamic diagram and the evaluation of the beam speed. The authors also thank the referees for their useful comments. The STEREO/WAVES investigation is a collaboration of the Observatoire de Paris, the University of Minnesota, the University of California Berkeley, and NASA/GSFC. The French contribution to this project is supported by the CNES and CNRS.

[64] Amitava Bhattacharjee thanks Peter Yoon and another reviewer for their assistance in evaluating this paper.

References

Acuña, M. H., D. Curtis, J. L. Scheifele, C. T. Russell, P. Schroeder, A. Szabo, and J. G. Luhmann (2007), The STEREO/IMPACT magnetic field experiment, *Space Sci. Rev.*, *136*, 203.

Bale, S. D., D. Burgess, P. J. Kellogg, K. Goetz, R. L. Howard, and S. J. Monson (1996), Phase coupling in Langmuir wave packets: Possible evidence of three-wave interactions in the upstream solar wind, *Geophys. Res. Lett.*, *23*, 109.

Bale, S. D., et al. (2008), The electric antennas for the STEREO/WAVES experiment, *Space Sci. Rev.*, *136*, 529.

Bardwell, S., and M. V. Goldman (1976), Three-dimensional Langmuir wave instabilities in type III solar radio bursts, *Astrophys. J.*, *209*, 912.

Bougeret, J. L., et al. (2007), S/WAVES: The radio and plasma wave investigation on the STEREO mission, *Space Sci. Rev.*, *136*, 487.

Budden, K. G. (1985), *The Propagation of Radio Waves: The Theory of Radio Waves of Low Power in the Ionosphere and Magnetosphere*, Cambridge Univ. Press, New York.

Cairns, I. H., and P. A. Robinson (1992), Theory for low-frequency modulated Langmuir wave packets, *Geophys. Res. Lett.*, *19*, 2187.

Cairns, I. H., and P. A. Robinson (1995), Ion acoustic wave frequencies and onset times during type III solar radio bursts, *Astrophys. J.*, *453*, 959.

Daubechies, I. (1990), The wavelet transform time-frequency localization and signal analysis, *IEEE Trans. Inf. Theory*, *36*, 961.

Dudok de Wit, T., and V. V. Krasnosel'Skikh (1995), Wavelet bicoherence analysis of strong plasma turbulence at the Earth's quasiparallel bow shock, *Phys. Plasmas*, *2*, 4307.

Ergun, R. E., et al. (2008), Eigenmode structure in solar-wind Langmuir waves, *Phys. Rev. Lett.*, *101*(5), doi:10.1103/PhysRevLett.101.051101.

Farge, M. (1992), Wavelet transforms and their applications to turbulence, *Annu. Rev. Fluid Mech.*, *24*, 395.

Ginzburg, V. L., and V. V. Zheleznyakov (1958), On the possible mechanisms of sporadic solar radio emission (radiation in an isotropic plasma), *Sov. Astron., Engl. Transl.*, *2*, 653.

Gurnett, D. A., G. B. Hospodarsky, W. S. Kurth, D. J. Williams, and S. J. Bolton (1993), Fine structure of Langmuir waves produced by a solar electron event, *J. Geophys. Res.*, *98*, 5631.

Hoang, S., G. A. Dulk, and Y. Leblanc (1994), Interplanetary type 3 radio bursts that approach the plasma frequency: ULYSSES observations, *Astron. Astrophys.*, *289*, 957.

Hospodarsky, G. B., and D. A. Gurnett (1995), Beat-type Langmuir wave emissions associated with a type III solar radio burst: Evidence of parametric decay, *Geophys. Res. Lett.*, *22*, 1161.

Kellogg, P. J., K. Goetz, N. Lin, S. J. Monson, A. Balogh, R. J. Forsyth, and R. G. Stone (1992), Low frequency magnetic signals associated with Langmuir waves, *Geophys. Res. Lett.*, *19*, 1299.

Kellogg, P. J., K. Goetz, S. J. Monson, S. D. Bale, and M. Maksimovic (2007), Electric field and density measurements with STEREO-Swaves, *Eos Trans. AGU*, *88*(52), *Fall Meet. Suppl.*, Abstract SH33A-1098.

Kennel, C. F., F. V. Coroniti, F. L. Scarf, R. W. Fredricks, D. A. Gurnett, and E. J. Smith (1980), Correlated whistler and electron plasma oscillation bursts detected on ISEE-3, *Geophys. Res. Lett.*, *7*, 129.

Koga, D., and T. Hada (2003), Phase coherence of foreshock MHD waves: Wavelet analysis, *Space Sci. Rev.*, *107*, 495.

Krasnoselskikh, V. V., V. V. Lobzin, K. Musatenko, J. Soucek, J. S. Pickett, and I. H. Cairns (2007), Beam-plasma interaction in randomly inhomogeneous plasmas and statistical properties of small-amplitude Langmuir waves in the solar wind and electron foreshock, *J. Geophys. Res.*, *112*, A10109, doi:10.1029/2006JA012212.

Lagoutte, D., F. Lefeuvre, and J. Hanasz (1989), Application of bicoherence analysis in study of wave interactions in space plasma, *J. Geophys. Res.*, *94*, 435.

Lepping, R. P., et al. (1995), The wind magnetic field investigation, *Space Sci. Rev.*, *71*, 207.

Li, B., P. A. Robinson, and I. H. Cairns (2006), Numerical simulations of type-III solar radio bursts, *Phys. Rev. Lett.*, *96*, 14,5005.

Lin, R. P., D. W. Potter, D. A. Gurnett, and F. L. Scarf (1981), Energetic electrons and plasma waves associated with a solar type III radio burst, *Astrophys. J.*, *251*, 364.

Lin, R. P., W. K. Levedahl, W. Lotko, D. A. Gurnett, and F. L. Scarf (1986), Evidence for nonlinear wave-wave interactions in solar type III radio bursts, *Astrophys. J.*, *308*, 954.

Lin, R. P., et al. (1995), A three-dimensional plasma and energetic particle investigation for the wind spacecraft, *Space Sci. Rev.*, *71*, 125.

Nishikawa, K. (1968), Parametric excitation of coupled waves: II. Parametric plasmon-photon interaction, *J. Phys. Soc. Jpn.*, *24*, 1152.

Pecseli, H. L., J. Trulsen, A. Bahnsen, and F. Primdahl (1993), Propagation and nonlinear interaction of low-frequency electrostatic waves in the polar cap E region, *J. Geophys. Res.*, *98*, 1603.

Robinson, P. A. (1993), Stochastic-growth theory of Langmuir growth-rate fluctuations in type III solar radio sources, *Solar Phys.*, *146*, 357.

Robinson, P. A., A. J. Willes, and I. H. Cairns (1993), Dynamics of Langmuir and ion-sound waves in type III solar radio sources, *Astrophys. J.*, *408*, 720.

Sagdeev, R. Z., and A. A. Galeev (1969), *Nonlinear Plasma Theory*, Benjamin, New York.

Siu, K., J. Ann, J. Kihwan, L. Myoungho, S. Kunsoo, and K. Chon (2008), Statistical approach to quantify the presence of phase coupling using the bispectrum, *IEEE Trans. Biomed. Eng.*, *55*, 1512.

Smith, D. F. (1970), Towards a theory for type III solar radio bursts: I. Nature of the exciting agency, *Solar Phys.*, *15*, 202.

Soucek, J., T. Dudok de Wit, V. Krasnoselskikh, and A. Volokitin (2003), Statistical analysis of nonlinear wave interactions in simulated Langmuir turbulence data, *Ann. Geophys.*, *21*, 681.

Sturrock, P.A. (1964), Type III solar radio bursts, in *Proceedings of a Symposium Held at the Goddard Space Flight Center, Greenbelt, Maryland, October 28–30, 1963*, edited by W. N. Hess, p. 357, NASA, Washington, D. C.

Thejappa, G., and R. J. MacDowall (1998), Evidence for strong and weak turbulence processes in the source region of a local type III radio burst, *Astrophys. J.*, *498*, 465.

Thejappa, G., D. Lengyel-Frey, R. G. Stone, and M. L. Goldstein (1993), Evaluation of emission mechanisms at omega P E using ULYSSES observations of type III bursts, *Astrophys. J.*, *416*, 831.

Thejappa, G., D. G. Wentzel, and R. G. Stone (1995), Low-frequency waves associated with Langmuir waves in solar wind, *J. Geophys. Res.*, *100*, 3417.

Thejappa, G., R. J. MacDowall, E. E. Scime, and J. E. Littleton (2003), Evidence for electrostatic decay in the solar wind at 5.2 AU, *J. Geophys. Res.*, *108*(A3), 1139, doi:10.1029/2002JA009290.

Torrence, C., and G. P. Compo (1998), A practical guide to wavelet analysis, *Bull. Am. Meteorol. Soc.*, *79*, 61.

van den Berg, J. C. (Ed.) (1999), *Wavelets in Physics*, Cambridge Univ. Press, New York.

Van Milligen, B. P., E. Sánchez, T. Estrada, C. Hidalgo, B. Brañas, B. Carreras, and L. García (1995), Wavelet bicoherence: A new turbulence analysis tool, *Phys. Plasmas*, *2*, 3017.

Wild, J. P. (1950), Observations of the spectrum of high-intensity solar radiation at metre wavelengths: III. Isolated bursts, *Aust. J. Sci. Res., Ser. A*, *3*, 541.

Willes, A. J., and I. H. Cairns (2001), Mode conversion and reflection of Langmuir waves in an inhomogeneous solar wind, *Publ. Astron. Soc. Aust.*, *18*, 355.

Willes, A. J., S. D. Bale, and I. H. Cairns (2002), Evidence for Langmuir wave tunneling in the inhomogeneous solar wind, *J. Geophys. Res.*, *107*(A10), 1320, doi:10.1029/2002JA009259.

S. D. Bale, Physics Department and Space Sciences Laboratory, University of California, Berkeley, CA 94720, USA.

C. Briand, F. Califano, P. Henri, and A. Mangeney, LESIA, Observatoire de Paris, Université Paris Diderot, CNRS, UPMC, 5 Place Jules Hansen, F-92190 Meudon, France. (pierre.henri@obspm.fr)

K. Goetz, School of Physics and Astronomy, University of Minnesota, Minneapolis, MN 55455, USA.

M. Kaiser, NASA Goddard Space Flight Center, Code 674, Greenbelt, MD 20771, USA.